Coupled eighth-mode Substrate Integrated Waveguide Antenna: Small and Wideband with High-Body Antenna Isolation

S. Agneessens, *Member, IEEE*

***Abstract*—A novel antenna design for wideband operation is presented, consisting of a system of two coupled miniaturized eighth-mode resonant radiating cavities with a low-complexity feeding network. The design methodology relies on the virtual magnetic boundaries along the symmetry planes of a rectangular waveguide resonator, for size reduction, and frequency bifurcation of two tightly coupled resonators, for bandwidth enhancement. After discussing its operating principle, a prototype targeting wearable applications is designed, manufactured, and validated. Multiband operation is achieved with simultaneous coverage of the 2.4 GHz ISM band and the LTE-7 up- and downlink bands. Measurements in free-space and on-body scenarios validate the antenna's performance. A bandwidth of 414 MHz (16.2 %) is measured, as well as a maximal gain of 4.7 dBi. The directive patch-like radiation pattern and the ground plane topology lead to high body-antenna isolation and good on-body performance. Impedance bandwidth and radiation pattern remain stable when the antenna is worn by a person and bent around a cylinder to mimic deformation.**

***Index Terms*—Antennas, Substrate Integrated Waveguide (SIW), Wearable antenna, Textile antenna, Half-mode Substrate Integrated Waveguide (HMSIW), Eighth-mode Substrate Integrated Waveguide (EMSIW), electrically small antenna, wideband antenna.**

I. Introduction

WIRELESS technology continues to open up new fields, new applications and new consumer markets. This evolution is driven by societal needs in areas such as healthcare, public service, and defense. The long-anticipated fifth-generation wireless networks (5G), the Internet-of-Things, and wearable applications [1–3], continue to produce new opportunities as well as new challenges. They call for the development of novel concepts and re-evaluation of design approaches.

The wired/wireless interface, being the antenna, is an essential component in the overall system performance. It directly influences the systems' communication range and coverage, achievable data-rate, energy efficiency and battery life, etc. Therefore, in an engineering field where every dB counts, the performance of antennas cannot be neglected. In this respect, relevant antenna figures of merit for overall system performance are footprint, wide bandwidth, radiation efficiency and pattern, reliability, and flexible performance. Especially the miniaturization and integration within the product poses quite some challenges on the antenna side, as there are quite some trade-offs, with a big influence, to be made.

For wearable applications, there are special requirements and challenges, due to the proximity of the body [4–6]. Typically, a flexible, low-profile topology is desired for easy integration into the wearer's garment and robustness against potential adverse influence by the human body, which may cause frequency detuning and radiation absorption.

This manuscript presents a novel, wearable antenna topology, based on a system of tightly coupled miniaturized resonators. Magnetic-mode miniaturization techniques are leveraged to achieve a wideband, small size component, with excellent performance. The capacitive coupling between the individual elements enable the use of a low-complexity feeding network.

The development of Substrate Integrated Waveguide (SIW) technology has given way to many new exciting design options, as it enables the implementation of rectangular waveguides for the creation of high-performance (active and passive) microwave components [7] in planar form. Miniaturization approaches that rely on the symmetry of the modes offer attractive opportunities for antenna design. Many researchers have looked into the possibilities of half-mode antennas [8], [9], as well as quarter [10], [11], eighth [12], [13], 16^{th} [14] and even 64^{th} mode [15].

Partial-mode techniques are also applied to achieve compact filters[16–18]. Designs based on multiple resonators yield circularly-polarized and wideband antennas [19], [20]. These compact wideband antennas do, however, require a complex feeding network, which introduces additional losses, uncertainty and increases the complexity and cost.

To cope with design challenges related to wearables, a part of the antenna community has dedicated its efforts to designing high-performance textile antennas. Different options have been explored to achieve good performance, despite the presence of the body. Ultra-wideband design have been explored with very

Submission date: 17-aug-2017

S. Agneessens is with Ghent University - imec, IDLab, Department of Information Technology and CMST, Department of Electronics and Information Systems, Technologiepark-Zwijnaarde 15, 9052 Ghent, Belgium (e-mail:sam.agneessens@ugent.be)

S. Agneessens is a postdoctoral fellow of FWO-V.

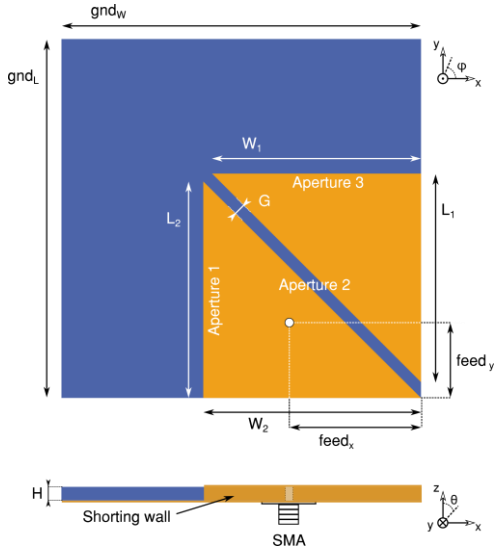

Fig. 1. The proposed novel antenna topology: a system of two coupled eighth-mode resonators excited by a low-complexity probe feed.
L1 = 29.5, W1 = 29.5, L2 = 30.5, W2 = 30.5, G = 1.41, gnd_w = 50, gnd_l = 50, H = 3.5, $feed_x$ = 18.5, feedy = 10.5 (all dimensions in mm).
Substrate parameters: ε_r =1.495, tan δ = 0.015

good body-antenna isolation & robustness [21], meta-materials and EBGs [22], RFID dedicated designs [23], [24].

SIW techniques have also been successfully applied to textile materials [8], [9], [11], [23], [25], [26], yielding antennas with very good on-body characteristics owing to the ability of SIW to shield radiation effectively from the human body. Given that textiles fabrics are difficult to integrate into typical electronic manufacturing processes, a lot of research efforts are concentrating on the development of new (textile-compatible) fabrication techniques for textile antennas, yielding very high accuracy & repeatability [27], and on the integration of active electronics [24]. Several approaches exist to implement SIW in textile materials, such as eyelets [8], [11], knitted vias [9], or e-textile sheets [28].

This manuscript presents the novel antenna topology that aims at combining high bandwidth, high-body antenna isolation, and a very low-complexity feeding structure in a small footprint. Which is achieved by relying on a coupled system of two miniaturized resonant cavities, operating at slightly different frequencies, that are fed by a single coaxial probe. The design process and the operating principle are explained in section II. The manufacturing process and design validation are discussed in sections III and IV.

II. Antenna Design Evolution and Operating Principle

A. *Wearable antenna design considerations*

Wearable antennas operate in very specific conditions. This needs to be taken into account early in the design process to achieve the best and most reliable performance. The design goals are:

- *Small footprint*
  Facilitates overall ease of integration into the wearable system and improves robustness and reliability, given the smaller probability of deformation.
- *Wideband operation*
  Important for two distinctly different reasons. First, sufficient bandwidth enables the antenna to cope with typical body-related frequency shifts due to bending or body-proximity. Second, more bandwidth allows a single antenna to cover multiple frequency bands corresponding to different applications, and to support more users, meaning it can be reused and it allows to keep the overall number of antennas low.
- *High body-antenna isolation*
  Required for energy efficiency, reliability, and user safety. Antennas that radiate a large amount of power towards the user are inadequate for many wearable applications as they dissipate power into the human body, which is not energy efficient from a system point of view, reduces the link budget, and has high likelihood of exceeding the Specific Absorption Rate (SAR) limits. Furthermore, a body-worn antenna with low body-antenna isolation will be less reliable as it is very susceptible to detuning.

B. *Design Evolution & Principle of Operation*

Based on the goals and requirements outlined in previous section, a dedicated design methodology is adopted to be able to combine small size, large bandwidth, and high body-antenna isolation.

The design evolution to achieve a novel antenna topology is shown in Fig. 2. Starting point is a closed cavity, with electric walls on all sides, resonating at its fundamental TE_{110} mode. Two miniaturized antennas can be distilled from this structure by relying on the virtual magnetic wall technique shown in Fig. 3 This technique takes advantage of the mode profile of the magnetic field. The tangential components vanish along the symmetry planes of the cavity, which behaves as a Perfect Magnetic Conductor (PMC). By bisecting the cavity and keeping an open boundary, a new, half-sized structure is obtained, with five electric walls and one magnetic wall. The mode profile and operating frequency remain quasi-identical to the original structure. Radiation now leaks through the open side, resulting in a half-mode antenna. This procedure can be repeated two more times, along the two remaining symmetry planes, leading to an antenna that operates at the same fundamental frequency, but occupies only $1/8^{th}$ of the area.

Two such antennas, with slightly different resonance frequencies, are combined on a common ground plane to form a two-antenna system, as shown in the final step of Fig. 2. The EM-fields in the cavities couple due to their close proximity, yielding wideband operation. An additional benefit of this coupling is that only one cavity (the main resonator) requires a feeding network, the second cavity acts as a coupled resonator (parasitic resonator).

Fig. 4. shows the electric field distribution inside the antenna, for the phase varying over one period. The two eighth-mode resonances, related to the TE_{110} mode, are excited inside each element. The phase of the parasitic element is leading by 90° (or lagging by 270°) with respect to that of the main resonator. The field magnitude inside the resonators depends on the

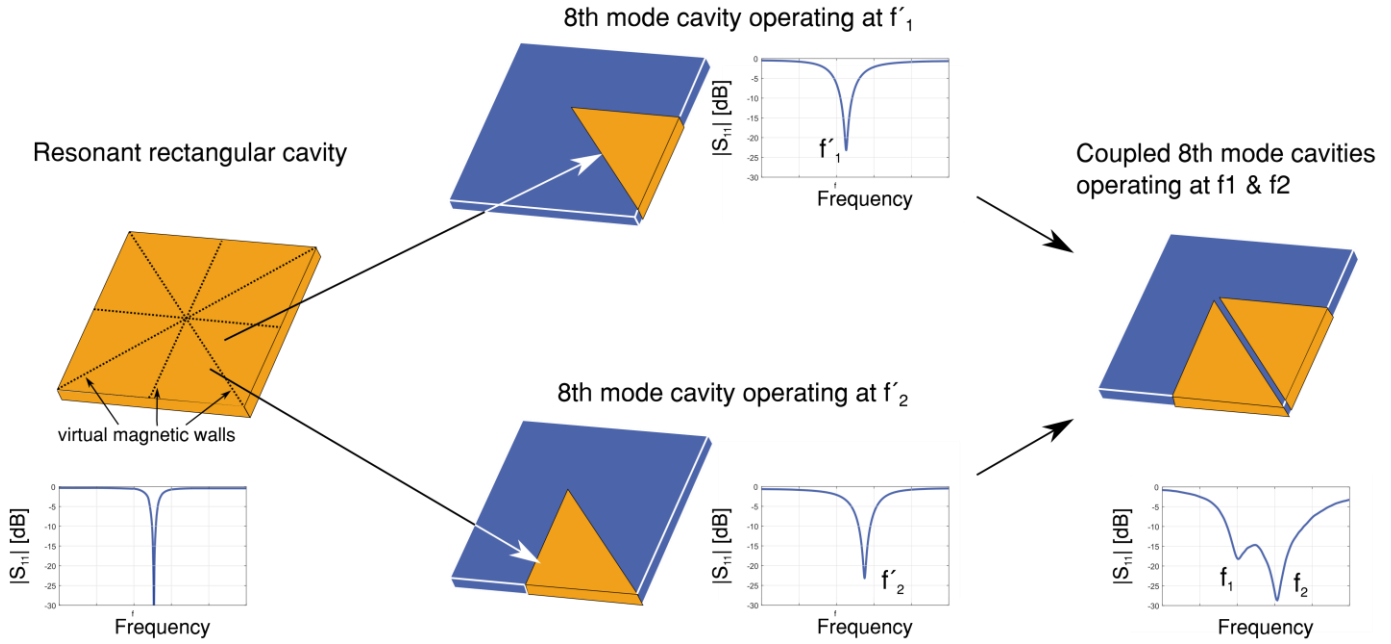

Fig. 2. Design evolution from left to right. Starting point is a resonant rectangular cavity. By bisected along virtual magnetic walls (where tangential components of the magnetic field vanish), two miniaturized resonant cavities are obtained. They operate at two closely spaced frequencies and occupy only 1/8th of the original resonator area. Through combination of the leaking resonators, a coupled-cavity system yields wideband operation in combination with a small footprint.

frequency. The largest field strengths, at any frequency *f* in the operating range, are found in the resonator that has its fundamental frequency closest to *f*.

The radiation originates from leakage through the open sidewalls along the x- and y-axis in Fig. 1. The tangential components of the electric field across these apertures combine in the far field. The contribution of the radiation through the gap between the two resonators is small compared to the contribution by the open walls. This is because the cavities need to be tightly coupled, and closely spaced, to obtain wideband operation.

Alternatively, the three slots can be seen as three radiating apertures (aperture 1: slot along y-axis of main cavity, aperture 2: slot between main and parasitic cavity, and aperture 3: opening along x-axis of parasitic cavity) and a cavity approximation (cfr. Microstrip patch antenna) can be assumed to understand the principle of radiation. The tangential component of the H-field is zero in all three apertures and only a tangential E-field with half-sine profile exists in these apertures. For aperture 1, the E-field has a component along $\mathbf{u_z}$. The field in aperture 3 is along $-\mathbf{u}_x$-$\mathbf{u}_y$ and lags 45° with respect to aperture 1. The field in the third and final aperture is also along $-\mathbf{u_z}$ and reaches its maximal strength 90° later than aperture 1.

The far field contribution of these fields over the apertures can be expressed by the $\mathbf{M}(\theta,\phi)$-vector, which is proportional to $\mathbf{e_{ap}} \times \mathbf{n}$. The $\mathbf{M}$-vector for aperture 1, $\mathbf{M}_1$ has a component along $-\mathbf{u}_y$, whereas $\mathbf{M_2}$ has a component along the $\mathbf{u}_x$-$\mathbf{u}_y$ direction, and $\mathbf{M_3}$ is solely along $\mathbf{u_x}$. The total $\mathbf{M}$-vector is the sum of these three individual contributions. Noting the 45° (approximately) phase difference between the field in the apertures, this results in a circular/elliptical polarization in the far field.

Extending the ground plane beyond the radiating apertures, leads to a more directional radiation pattern. The lower hemisphere (negative z-axis in Fig. 1) is effectively shielded from the radiation, resulting in high body-antenna isolation.

The relation between the fields in both resonators (strength & phase) can be used to tune the polarization of the antenna. With a phase difference of 90 ° and equal field strength in both cavities, perfect circular polarization could be obtained. Right-hand or left-hand circular polarization can be selected by choosing the main resonator. If the bottom cavity is fed (like in Fig. 1), the polarization is left-handed. Right-handed polarization is achieved by feeding the other cavity. The circular polarization bandwidth for antennas relying on two modes is, generally speaking, smaller than its impedance bandwidth. In the design presented here the choice is made to maximize the impedance bandwidth at the expense of polarization purity.

The main resonator can be excited by using an SMA connector. The connector ground is connected to the bottom of the cavity. The signal pin to the top of the main resonator. The SMA connector and the cavity form a current loop (SMA signal pin, cavity top, side wall, cavity bottom, SMA ground) that effectively couples to the magnetic field of the resonators fundamental TE_{110} mode. Other feeding techniques can be used as well, such as microstrip inset, aperture coupling, and coupling to the magnetic or electric field of a substrate integrated waveguide feed network.

C. Sensitivity analysis

A sensitivity analysis and parameter study are conducted to provide insight into the most crucial design parameters and into the sensitivity to manufacturing tolerances. This study is performed by using a finalized wearable antenna design, with dimensions in the caption of Fig. 1. covering the 2.4 GHz ISM (2.4 – 2.4835 GHz) and LTE-7 bands (uplink: 2.5 – 2.57 GHz, downlink: 2.62 – 2.69 GHz). The parameters discussed below are the most crucial to the design performance, meaning that

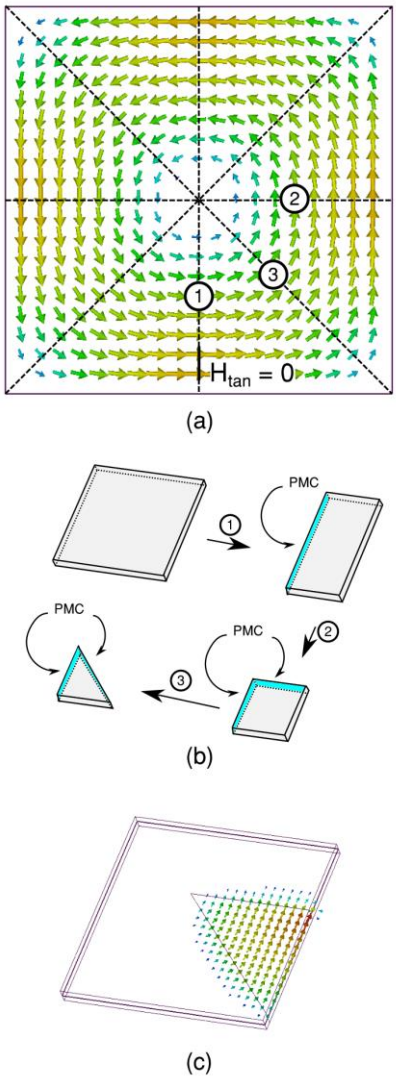

Fig. 3. Half-mode miniaturization. (a) Symmetry planes of a rectangular cavity. The tangential component of the magnetic field is zero, mimicking a Perfect Magnetic Conductor (PMC). (b) The cavity can be miniaturized by removing half of the cavity. The open boundary acts as a virtual magnetic wall. This can be repeated for each remaining symmetry plane. (c) An 8th mode cavity has a much smaller footprint, but the same operating frequency and mode distribution as the original cavity.

their variations will have the largest influence on impedance matching and radiation characteristics.

1) Cavity size

The selection of the resonance frequencies is straightforward. They depend on the size of the cavity. The well-known waveguide formula [29] can be used:

$$f_{110} = \frac{c}{2\pi\sqrt{\mu_r \varepsilon_r}}\sqrt{\left(\frac{\pi}{a}\right)^2 + \left(\frac{\pi}{b}\right)^2} \qquad (1)$$

with a and b are the dimensions of the cavity in the x and y-directions. This formula shows the inverse relation between frequency and cavity size. It should be noted that the fringing fields will alter (lower) the effective permittivity (due to their presence in the air) and hence increase the operating frequency.

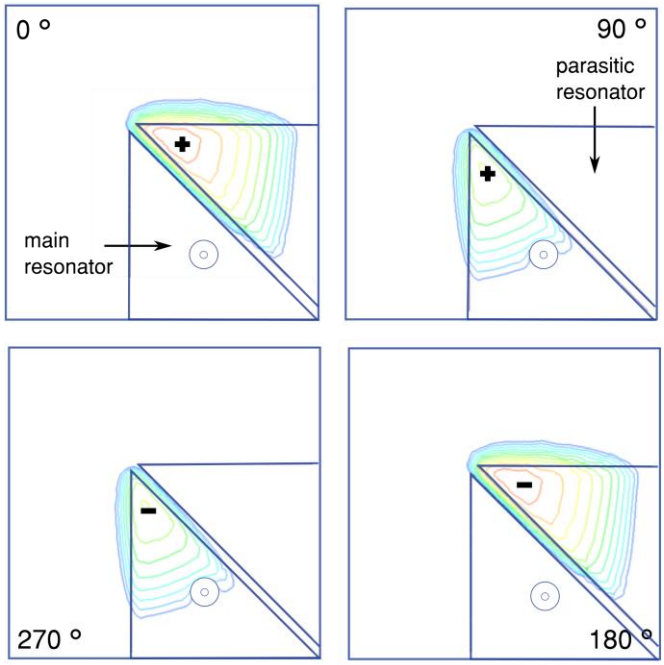

Fig. 4. Electric-field magnitude throughout one frequency cycle at the 2.45 GHz. Both patches operate in the TE_{110}-mode (reduced size), with a phase difference of approximately 90 degrees between both resonators.

2) Coupling between resonant cavities

The coupling between both cavities is a significant factor of influence. Tight coupling results in bifurcation of the resonant modes, i.e. the resonant frequencies will split up and shift apart. It is advised to fine-tune this effect in simulation. Three parameters are of major influence: substrate height, substrate permittivity, and gap size. These parameters influence whether the E-field remains confined to the main cavity or whether it couples easily from one cavity to the other.

Increasing substrate height or lowering the substrate's permittivity results in a less confined E-field (or larger fringing field), which increases the coupling between the cavities. An identical effect is obtained by reducing the gap size between both cavities. The proximity coupling, which is capacitive in this case, is -as expected- improved by placing the cavities closer to each other.

3) Ground plane size

In an ideal case, the ground plane would be infinitely large, as this would lead to very high-body antenna isolation, providing low SAR values and avoiding frequency detuning and radiation pattern deformation. For wearable applications, a small ground plane is not realistic. On the contrary, for integration ease, a smaller overall footprint is a prerequisite. The reduction of the ground plane directly influences the flow of current and, hence, the fringing field. Decreasing this parameter makes the radiation pattern less directive.

4) Feed position

The position of the feed determines the coupling between the EM-field in the primary cavity and the feedline. The position of the feed should be chosen carefully, such that the impedance of the resonator locally matches that of the feed line. This is comparable with the design procedure of a microstrip patch antenna.

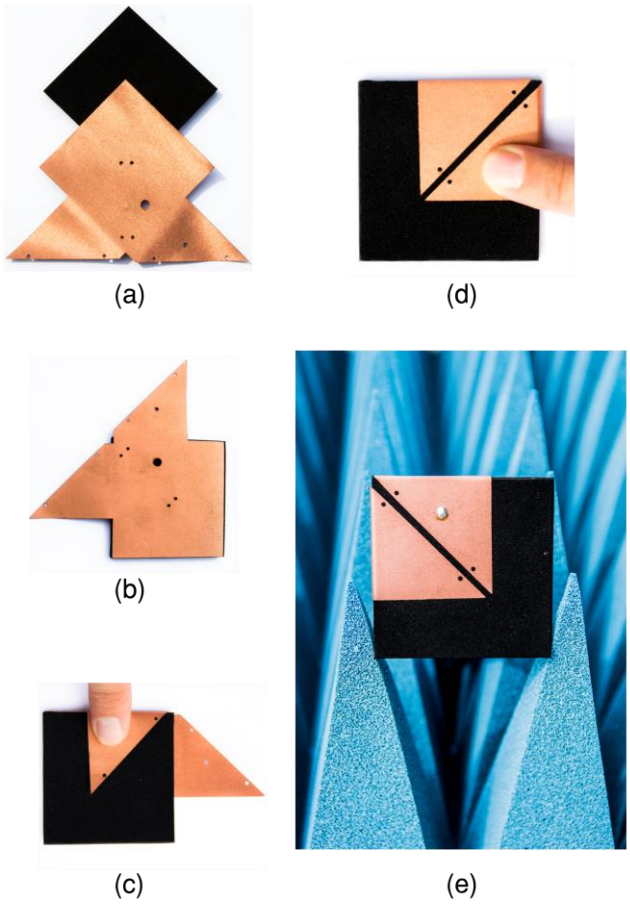

Fig. 5. Assembly of the wearable antenna. (a) Substrate and e-textile are patterned with laser cutter. The conductive parts are made from a single sheet and small alignment holes in substrate and conductor are used to facilitate reliable manufacturing. (b) The ground plane is glued to the back side of the substrate. (c) The first resonator is created by folding the flap over the substrate. (d) The second resonator is realized accordingly. (f) Photograph of the finalized antenna.

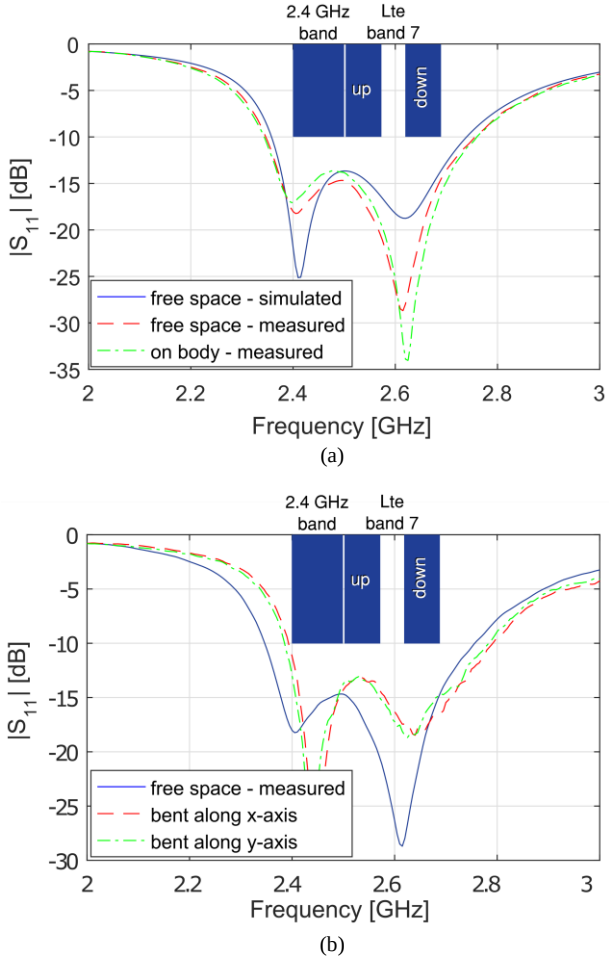

Fig. 6. The antenna shows good impedance matching to a 50 Ω reference impedance under the different operating conditions. (a) Free space (simulated and measured) and on-body (measured) agree well, and (b) stable performance is observed when the antenna is bent around a cylinder with radius of 9 cm.

III. Manufacturing Process and Considerations

A prototype for wearable applications was manufactured with a final volume of 50 x 50 x 3.5 mm^3 (dimensions in caption of Fig. 1. Textile materials are selected to obtain a flexible antenna that can easily be integrated into the wearer's garments. Furthermore, the chosen materials have a large impact on the performance of wearable designs. To maximize the radiation efficiency of the antenna, a substrate with low moisture-regain and low losses is essential, in addition to an e-textile with low sheet resistance. Closed-cell expanded rubber, typically found in firefighter gear, is used as a substrate (ε_r *=1.495, tan* δ *= 0.015*) and a copper-plated taffeta polyester (σ *= 3e5 S/m*), which is tightly woven for good electrical contact between the fibers, and which has a coating to prevent oxidation is used to realize the conductive sheets of the antenna.

The patterning of the textiles is performed by laser cutting with spot size of 100 µm. To minimize misalignment, the top and bottom metal layers are cut from a single e-textile sheet, which is folded around the substrate. This is an easy and cost-effective way to realize the electric walls [28]. Alternatively, the electric boundary can be implemented by using eyelets that act as vias. The dimensions of the cavities should then be adjusted to that of the equivalent substrate integrated waveguide [7].

The assembly process and finalized prototype are displayed in Fig. 5. Small holes are used to accurately align the two resonators. Given their small size (radius < 0.5 mm), there is negligible influence on the antenna performance. This was validated by simulations before manufacturing. Thermally activated glue was used to assemble the substrate and conductor layers.

IV. Design Validation

The design is validated for two different operating conditions. In free space, the general performance of the antenna is measured and compared to simulation values. While on-body measurements provide knowledge about how robust (and reliable) the antenna is near the human body.

A. Stand-alone performance

Free-space conditions are achieved by placing the antenna in the anechoic room. Scattering parameters are measured using a Keysight PNA-X to check the impedance matching bandwidth w.r.t. a 50 Ω reference impedance. Fig. 6.a. shows the simulated

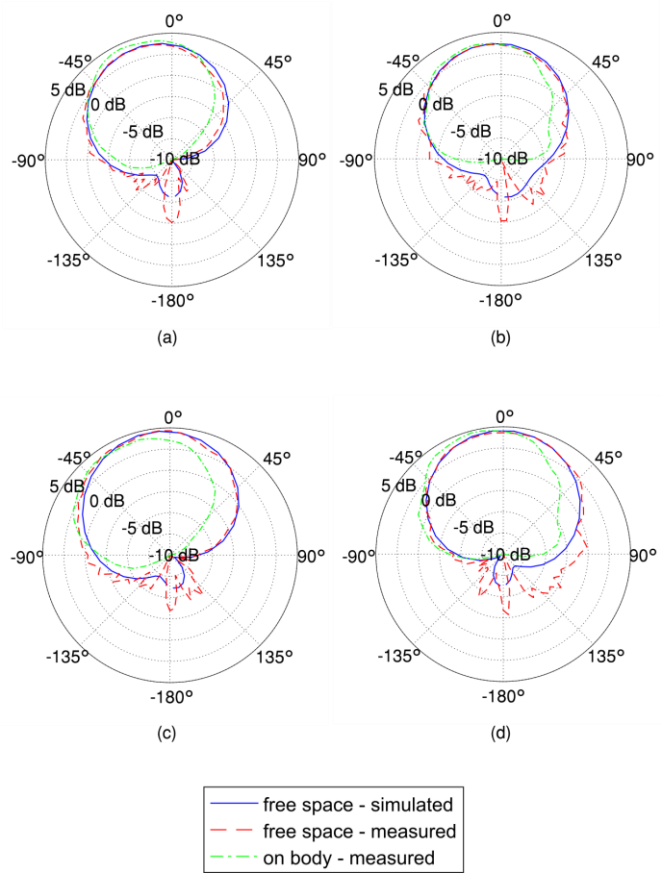

Fig. 7. Radiation pattern of the proposed antenna. The simulated and measured free-space total gain and measured on-body gain are shown in (a) the horizontal (xz) plane at 2.45 GHz, (b) the vertical (yz) plane at 2.45 GHz, (c) the horizontal (xz) plane at 2.655 GHz and (d) the vertical (yz) plane at 2.655 GHz

and measured reflection coefficient of the antenna. The measured bandwidth equals 414 MHz (16.2 %), which is somewhat larger than the simulated value of 385 MHz (15.2 %). This difference can be attributed to the uncertainty on the gap width (due to the manual assembly) and to variations of material properties (such as deviation in permittivity of the textile substrate or substrate heigth).

The measured bandwidth of the proposed coupled 8th-mode antenna is more than three times that of the quarter-mode SIW antenna reported in [11], which is fabricated from identical materials and occupies a slightly larger volume.

Full 3D pattern was measured to validate the radiation performance at the center frequency of the 2.4 GHz ISM band (2.45 GHz.) and the LTE-7 downlink band (2.655 GHz). Fig. 7. shows the horizontal and vertical cuts of the far-field pattern.

The measured and simulated radiation patterns at both frequencies agree well. At 2.45 GHz, the maximal gain is 3.8 dBi (3.9 dBi simulated) and 4.7 dBi (4.6 dBi simulated) at 2.655 GHz. Fig. 8 shows the measured and simulated gain variation as a function of frequency. The increasing gain w.r.t. frequency can be attributed to the fact that at lower frequencies the radiation originates only from the first resonant cavity, while at higher frequencies both resonators contribute to the far field, this in addition to the increased conductor losses. The measured antenna efficiency equals 67% (70 % simulated) and 82 % (80 % simulated) at the high and lower frequency points,

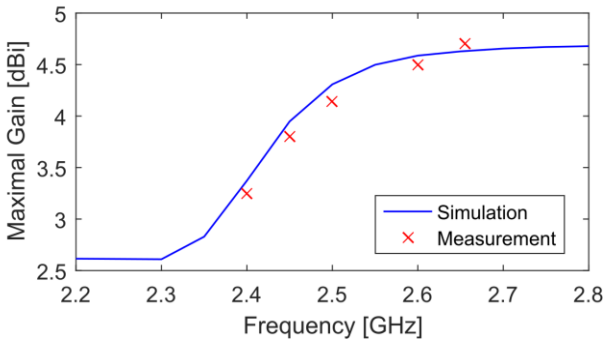

Fig. 8. Simulated and measured maximal gain of the proposed antenna

respectively. In the horizontal and vertical plane, the 3dB half-beam width equals approximately 35 ° and 50 ° at 2.45 GHz, and 40 ° and 50 ° at 2.655 GHz. The shape of the radiation pattern resembles that of the well-known microstrip patch antenna.

From the discussion on the radiation mechanism, the antenna is expected to exhibit elliptical polarization. Fig. 9 shows the left-handed & right-handed circular polarized components of the design. It can be seen that the antenna's polarization is indeed left-handed elliptical, with an AR of 5 dB and 17 dB at 2.45 GHz and 2.655 GHz, respectively.

B. On-body performance

Impedance matching deterioration and frequency detuning are commonly caused by proximity of the human body. Reflection coefficient measurements, shown in Fig. 6.a. when the antenna is placed on-body reveal stable performance. Additional near-field absorption and capacitive coupling typically caused by the human body is avoided by the use of a ground-plane topology.

Resilience against deformation is tested by bending the antenna around a cylinder of radius comparable to that of a human leg (9 cm). The measured reflection coefficient, in Fig. 6.b., shows slight detuning, with an upward frequency shift. The excess bandwidth of the original design is sufficient to cope with this shift and to maintain operation in both bands. Bending of the antenna around the cylinder results in negligible changes in the simulated gain and efficiency.

Fig. 7. also shows the measured radiation pattern when the antenna is placed on the chest of a test subject with a BMI of 22.5. The maximal gain is 4.5 dBi at 2.45 GHz and 4.8 dBi at 2.655 GHz. The backward radiation is almost entirely blocked by the wearer. While antenna gain for directions "away from the body" remains virtually unchanged, the gain for radiation towards the body is virtually zero.

This body absorption could potentially be harmful and result in health issues when the antenna is used as a transmitter. To this end, a Specific Absorption Rate simulation is performed with the antenna placed 2 mm above the three-layer human-body model [8]. The SAR values are calculated in a worst-case scenario, with the antenna transmitting the maximal equivalent isotropic radiated power (EIRP) allowed in each frequency band. The resuls are well below the limit of 1.6 mW/g, with 0.24 mW/kg at 2.45 GHz and 0.26 mW/g at 2.535 GHz. The SAR performance can further be improved by increasing the ground plane size.

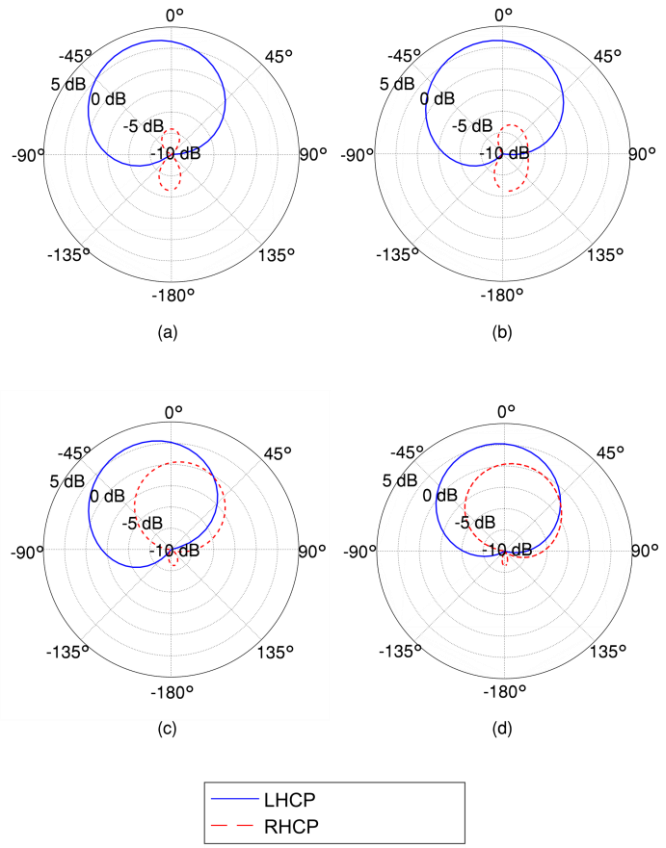

Fig. 9. Simulated LHCP and RHCP components of the antenna gain at (a) the horizontal (xz) plane at 2.45 GHz, (b) the vertical (yz) plane at 2.45 GHz, (c) the horizontal (xz) plane at 2.655 GHz and (d) the vertical (yz) plane at 2.655 GHz

V. Conclusions and Outlook

A novel antenna topology is presented, which combines - often conflicting- properties: small footprint, wide bandwidth, low-complexity, and reliable performance near the human body. Its operation is based a system of two miniaturized eighth-mode coupled resonators fed by a very low-complexity probe feed.
High body-antenna isolation is achieved through the directional radiation pattern and the use of a ground plane, resulting in stable and reliable on-body performance.
A prototype covering the 2.4 GHz ISM band and both the LTE-7 up and downlink band was investigated, manufactured and validated in stand-alone and on-body scenarios. The antenna's measured bandwidth equals 414 MHz or 16.2 %. The measured free-space antenna gain is 3.8 dBi (2.4 GHz ISM band) and 4.7 dBi (LTE 7 downlink), comparing well with the simulated values of 3.9 dBi and 4.6 dBi. Additional measurements were conducted for on-body performance evaluation. Virtually no impedance matching detuning or degradation was observed when the antenna is placed on the chest. Bending tests mimicking bending around a leg, also revealed stable performance under these adverse conditions. Finally, the Specific Absorption Rate was calculated in both operating bands. It was found to be well below the legal limit, with 0.24 W/kg (2.4 GHz ISM band) and 0.26 W/kg (LTE 7 uplink), showing that the antenna's radiation poses no potential harm to the user.

The presented antenna is a good candidate for wearable applications such as multi-band WBAN, or body-worn multi-antenna systems, such as MIMO, wearable radar, or other beamforming applications.

Acknowledgment

I would like to acknowledge H. Rogier for proof reading the manuscript, T. Deckmym for the pictures and J. Nielandt for his assistance with the measurements.

References

[1] N. F. M. Aun, P. J. Soh, A. A. Al-Hadi, M. F. Jamlos, G. Vandenbosch, and D. Schreurs, "5G Technologies: Recent Developments and Future Perspectives for Wearable Devices and Antennas," *IEEE Microwave Magazine*, vol. 18, 2017.

[2] J. Gubbi, R. Buyya, S. Marusic, and M. Palaniswami, "Internet of Things (IoT): A vision, architectural elements, and future directions," *Future Gener. Comp. Sy.*, vol. 29, no. 7, pp. 1645–1660.

[3] *Worldwide Wearables Market to Nearly Double by 2021, According to IDC*. IDC press release: http://www.idc.com/getdoc.jsp?containerId=prUS42818517.

[4] P. Salonen, Y. Rahmat-Samii, and M. Kivikoski, "Wearable antennas in the vicinity of human body," in *Antennas and Propagation Society International Symposium*.

[5] C. Hertleer, A. Van Laere, H. Rogier, and L. Van Langenhove, "Influence of relative humidity on textile antenna performance," *Textile Research Journal*, vol. 80, no. 2, pp. 177–183, 2010.

[6] F. Boeykens, H. Rogier, and L. Vallozzi, "An efficient technique based on polynomial chaos to model the uncertainty in the resonance frequency of textile antennas due to bending," *IEEE Trans. Antennas Propagat.*, vol. 62, no. 3, pp. 1253–1260, 2014.

[7] M. Bozzi, A. Georgiadis, and K. Wu, "Review of substrate-integrated waveguide circuits and antennas," *IET Microwaves, Antennas & Propagation*, vol. 5, no. 8, pp. 909–920, 2011.

[8] S. Agneessens and H. Rogier, "Compact Half Diamond Dual-Band Textile HMSIW On-Body Antenna," *IEEE Transactions on Antennas and Propagation*, vol. 62, no. 5, pp. 2374–2381, May 2014.

[9] T. Kaufmann and C. Fumeaux, "Wearable Textile Half-Mode Substrate-Integrated Cavity Antenna Using Embroidered Vias," *IEEE Antennas Wirel. Propag. Lett.*, vol. 12, pp. 805–808, 2013.

[10] C. Jin, R. Li, A. Alphones, and X. Bao, "Quarter-mode substrate integrated waveguide and its application to antennas design," *IEEE Transactions on Antennas and Propagation*, vol. 61, no. 6, pp. 2921–2928, 2013.

[11] S. Agneessens, S. Lemey, T. Vervust, and H. Rogier, "Wearable, Small, and Robust: The Circular Quarter-Mode Textile Antenna," *IEEE Antenn. Wireless Propag. Lett.*, vol. 14, pp. 1482–1485, 2015.

[12] S. Sam and S. Lim, "Electrically small eighth-mode substrate-integrated waveguide (EMSIW) antenna with different resonant frequencies depending on rotation of complementary split ring resonator," *IEEE Transactions on Antennas and Propagation*, vol. 61, no. 10, pp. 4933–4939, 2013.

[13] K. Kim and S. Lim, "Miniaturized Circular Polarized TE _10-Mode Substrate-Integrated-Waveguide Antenna," *IEEE*

Antennas and Wireless Propagation Letters, vol. 13, pp. 658–661, 2014.

[14] A. Azad and A. Mohan, "Sixteenth-mode substrate integrated waveguide bandpass filter loaded with complementary split-ring resonator," *Electronics Letters*, vol. 53, no. 8, pp. 546–547, 2017.

[15] S. Choudhury and A. Mohan, "Electrically small 64th-mode substrate-integrated waveguide monopole antenna," *Electronics Letters*, vol. 52, no. 8, pp. 580–581, 2016.

[16] C. Jin and Z. Shen, "Compact triple-mode filter based on quarter-mode substrate integrated waveguide," *IEEE Transactions on Microwave Theory and Techniques*, vol. 62, no. 1, pp. 37–45, 2014.

[17] P. Li, H. Chu, and R.-S. Chen, "Design of Compact Bandpass Filters Using Quarter-Mode and Eighth-Mode SIW Cavities," *IEEE Transactions on Components, Packaging and Manufacturing Technology*, vol. 7, no. 6, pp. 956–963, 2017.

[18] S. Moscato, C. Tomassoni, M. Bozzi, and L. Perregrini, "Quarter-mode cavity filters in substrate integrated waveguide technology," *IEEE Transactions on Microwave Theory and Techniques*, vol. 64, no. 8, pp. 2538–2547, 2016.

[19] Z. Wang, Y. Ran, Y. Peng, Y. Li, and Y.-Q. Sun, "Broadband Circularly Polarized Antenna Based on Quarter-Mode Substrate Integrated Cylindrical Cavity Subarray," *Progress In Electromagnetics Research Letters*, vol. 54, pp. 61–66, 2015.

[20] C. Jin, Z. Shen, R. Li, and A. Alphones, "Compact Circularly Polarized Antenna Based on Quarter-Mode Substrate Integrated Waveguide Sub-Array," *IEEE Transactions on Antennas and Propagation*, vol. 62, no. 2, pp. 963–967, Feb. 2014.

[21] P. B. Samal, P. J. Soh, and G. A. Vandenbosch, "UWB all-textile antenna with full ground plane for off-body WBAN communications," *IEEE Transactions on Antennas and Propagation*, vol. 62, no. 1, pp. 102–108, 2014.

[22] S. Yan, P. J. Soh, and G. A. Vandenbosch, "Compact all-textile dual-band antenna loaded with metamaterial-inspired structure," *IEEE Antennas and Wireless Propagation Letters*, vol. 14, pp. 1486–1489, 2015.

[23] T. Kaufmann, D. C. Ranasinghe, M. Zhou, and C. Fumeaux, "Wearable Quarter-Wave Folded Microstrip Antenna for Passive UHF RFID Applications," *Int J Antennas Propag*, pp. 1–11, 2013.

[24] S. Lemey, S. Agneessens, P. Van Torre, K. Baes, J. Vanfleteren, and H. Rogier, "Wearable Flexible Lightweight Modular RFID Tag With Integrated Energy Harvester," *IEEE Trans. Microw. Theory Techn.*, vol. 64, no. 7, pp. 2304–2314, Jul. 2016.

[25] R. Moro, S. Agneessens, H. Rogier, and M. Bozzi, "Wearable Textile Antenna in Substrate Integrated Waveguide Technology," *IET Electron. Lett.*, vol. 48, no. 16, pp. 985–987.

[26] R. Moro, S. Agneessens, H. Rogier, A. Dierck, and M. Bozzi, "Textile Microwave Components in Substrate Integrated Waveguide Technology," *IEEE Trans. Microw. Theory Techn.*, vol. 63, no. 2, pp. 422–432, Feb. 2015.

[27] A. Kiourti and J. L. Volakis, "High-Geometrical-Accuracy Embroidery Process for Textile Antennas With Fine Details," *IEEE Antennas and Wireless Propagation Letters*, vol. 14, pp. 1474–1477, 2015.

[28] S. Yan, P. J. Soh, and G. A. Vandenbosch, "Dual-band textile MIMO antenna based on substrate-integrated waveguide (SIW) technology," *IEEE Transactions on Antennas and Propagation*, vol. 63, no. 11, pp. 4640–4647, 2015.

[29] D. M. Pozar, "Microwave Engineering." Wiley, 2012.